

# Chapter 2

## Advances in 3D Numerical Simulation of Viscous and Viscoelastic Mixing Flows

Kiran V. Vyakaranam and Jozef L. Kokini

### 2.1 Introduction

Mixing processes in the food industry often involve highly viscous and viscoelastic fluids like wheat flour dough, pastes, batters, and syrups. The design of mixing equipment, whether batch or continuous, is aimed at achieving a well-mixed and blended product with a consistent rheological character. Design of mixing equipment also involves devising guidelines for scale-up of mixing devices and their comparison in terms of mixing efficiency, especially when batch mixers are to be replaced by continuous mixing equipment. A well-designed mixing process could result in the blending of ingredients, improvement of rate of heat transfer, facilitation of chemical reactions, creation of structure, addition of energy to create or break molecular bonds, etc. In order to evaluate the efficiency of a mixer design in performing these operations, a kinematic analysis of the process can be made wherein the mixing mechanisms are characterized as “dispersive” or “non-dispersive” (or extensive) (Wang and Manas-Zloczower 2001). Dispersive mixing is quantified by elongational flow and shear stress, which aid in the breakup of cohesive particles like droplets, bubbles, or solid agglomerates. Non-dispersive mixing includes the spatial separation and rearrangement of an initially cohesive cluster of particles (distributive mixing) or the laminar stretching and folding of the material elements, resulting in a homogeneous distribution (Meijer and Janssen 1994).

Mixing devices currently used in process industries are either batch or continuous. These devices vary in the design of the impellers, kneading blocks, and/or static mixing elements, depending on the material used, the throughput requirements, and the specific aim of the mixing process, for example, the stretching and folding of material or dispersion of ingredients. Examples of batch mixers include

---

K.V. Vyakaranam

Department of Food Science, Rutgers University, New Brunswick, NJ 08901, USA

J.L. Kokini (✉)

Department of Food Science and Human Nutrition, College of ACES, University of Illinois at Urbana Champaign, Urbana, IL 61801, USA

e-mail: kokini@uiuc.edu

the stirred tank reactors with Rushton impellers and dough kneaders like the Brabender farinograph and Banbury mixers, while examples of continuous mixers include the twin-screw/single-screw extruders and static mixers fitted with varying mixing elements (e.g., Kenics mixer). While the evaluation of flow and subsequent mixing parameters can be done using visualization techniques like particle image velocimetry (PIV) and laser doppler anemometry (LDA), it is often not practical to optimize the design of such large mixing devices (i.e., to industrial scale) through experimental trial-and-error analysis. Numerical simulation techniques thus have proven to be a viable, nonintrusive, and cost-effective alternative tool that can optimize the design of complex mixer geometries through analysis of the flow field and mixing parameters.

Research involving numerical simulation of mixing flows has been under steady development, ranging in the beginning from the simplest 2D problems to more realistic 3D mixer geometries. In this chapter we initially discuss the basic ideas behind numerical simulation of mixing flows, using the finite element method (FEM) and the governing equations and theoretical measures of the mixing process. A review is then presented of the recent work done in analyzing flow and mixing of viscous and viscoelastic fluids in various batch and continuous mixing geometries using FEM simulations.

## 2.2 Theoretical Measures of Mixing

There are several measures used to quantify distributive and dispersive mixing, as well as laminar stretching and folding of the material. During mixing of two components (distributive mixing) the homogeneity of the mixture can be quantified through the scale of segregation,  $S(t)$ , which is a measure of the binomial distribution of the components and is calculated as

$$S(t) = \int_0^{\zeta} R(r, t) dr \quad (2.1)$$

where  $R(|r|)$  is a correlation coefficient that gives the probability of “ $M$ ” pairs of material points in the mixer separated by a distance  $|r|$  having the same concentration,

$$R(|r|) = \frac{\sum_{j=1}^M (c'_j - \bar{c}) \cdot (c''_j - \bar{c})}{MS^2} \quad (2.2)$$

The parameter  $S(t)$  gives an indication of the average size of the segregated regions but cannot detect local defects in the flow.

When a cluster of material points is distributed, the difference between the actual distribution and the ideal distribution of the material points is called the “pair-wise distribution index” or the “cluster distribution index”  $\varepsilon$ , and is calculated as

$$\varepsilon = \frac{\int_0^\infty [c(r) - c(r)_{\text{ideal}}]^2 dr}{\int_0^\infty [c(r)_{\text{ideal}}]^2 dr}, \quad (2.3)$$

where  $c(r)$  is the coefficient of the probability density function and the value of index  $\varepsilon$  varies from 0 (ideal distribution) to 1 (no distribution) (Connelly and Kokini 2007).

The efficiency of a mixing flow to stretch and fold the material can be studied using a kinematic approach wherein the deformation of infinitesimal material lines and surface elements is tracked (Ottino 1989).

If the motion of the fluid is described by  $\mathbf{X} = \chi(\mathbf{X}, t)$ , and the deformation of an infinitesimal material line by  $d\mathbf{x} = \mathbf{F} \cdot d\mathbf{X}$ , then the length of stretch  $\lambda$  can be defined in terms of the strain as

$$\lambda = \lim_{|d\mathbf{x}| \rightarrow 0} \frac{|d\mathbf{x}|}{|d\mathbf{X}|} \quad (2.4)$$

and a local instantaneous efficiency of mixing given by

$$e_\lambda(\mathbf{X}, \mathbf{M}, t) = \frac{D \ln \lambda / Dt}{(\mathbf{D} : \mathbf{D})^{1/2}} \quad (2.5)$$

where  $\mathbf{M} = \frac{d\mathbf{x}}{|d\mathbf{X}|}$  and  $\mathbf{D}$  represents the rate of strain tensor with a magnitude  $(\mathbf{D} : \mathbf{D})^{1/2}$ .

If the material is an incompressible Newtonian fluid, the local instantaneous efficiency will be the fraction of dissipated energy used to stretch the material, ranging between  $-1$  and  $1$ . The time averaged efficiency  $\langle e_\lambda \rangle$  given in (2.6) provides information on the nature of reorientation (stretching and folding) of the flow. Flows with no reorientation will have  $\langle e_\lambda \rangle$  decaying with time as  $t^{-1}$ , whereas  $\langle e_\lambda \rangle$  tending toward a constant value would indicate a flow with strong reorientation (Ottino 1989).

$$\langle e_\lambda \rangle(\mathbf{X}, \mathbf{M}, t) = \frac{1}{t} \int_0^t e_\lambda(\mathbf{X}, \mathbf{M}, t') dt' \quad (2.6)$$

Similar efficiency in stretching of an infinitesimal area element can also be evaluated. In a chaotic time-periodic flow, the arithmetic and geometric means of the length of stretch,  $\lambda$ , grow exponentially and can be represented as

$$\bar{\lambda} \approx \alpha \cdot e^{\Theta n}, \quad \langle \lambda \rangle \approx \alpha \cdot e^{\Lambda n} \quad (2.7)$$

where  $n$  is the number of periods of revolutions and  $\Theta$  and  $\Lambda$  are the topological entropy exponent and Lyapunov exponent, respectively. While topological entropy is a measure of the mixing rate in chaotic regions of flow, the Lyapunov exponent measures the rate of elongation or stretching (Muzzio et al. 2000; Zalc et al. 2002a).

Dispersive mixing involves breakup of agglomerates and drops in flow, caused by stresses large enough to overcome the cohesive or interfacial forces that tend to keep the agglomerate or the drop intact. The mechanical stress required for breakup depends on the type of flow, with pure elongation or irrotational flows being more effective than flows with a rotational component (Grace 1982; Bentley and Leal 1986). A dispersive “mixing index”  $\lambda_{MZ}$ , which quantifies the relative strength of the pure elongational flow component, can be defined as

$$\lambda_{MZ} = \frac{|\mathbf{D}|}{|\mathbf{D}| + |\mathbf{\Omega}|} \quad (2.8)$$

where  $\mathbf{D}$  and  $\mathbf{\Omega}$  are the rate of deformation and vorticity tensors, respectively (Yang and Manas-Zloczower 1992).  $\lambda_{MZ}$  ranges from 0 for pure rotation to 0.5 for simple shear, and to 1.0 for pure elongation. The Manas-Zloczower mixing index (as defined above) is not frame-invariant. However, several other frame-invariant flow-type indices were found to be computationally difficult to evaluate due to the requirement of higher-mesh densities in the simulation; and provided information similar to that of the non-frame-invariant index (Wang and Manas-Zloczower 2001; Connelly 2004).

### 2.3 Governing Equations for Calculation of Flow

The velocity and pressure distributions for an incompressible and isothermal fluid flow are calculated from the Navier–Stokes equations of mass and momentum conservation:

$$\nabla \cdot \mathbf{v} = 0 \quad (2.9)$$

$$\nabla \cdot \boldsymbol{\sigma} + \rho \mathbf{f} = \rho \left( \frac{\partial \mathbf{v}}{\partial t} + \mathbf{v} \cdot \nabla \mathbf{v} \right) \quad (2.10)$$

where  $\rho$  is the fluid density and  $\mathbf{f}$  is the external body force per unit mass.

The stress tensor  $\boldsymbol{\sigma}$  given in (2.10) incorporates the isotropic pressure ( $P$ ) and extra stress tensor ( $\mathbf{T}$ ), defined as

$$\boldsymbol{\sigma} = -P\mathbf{I} + \mathbf{T} \quad (2.11)$$

An additional energy conservation equation has to be solved in the case of a non-isothermal flow to obtain the temperature distribution:

$$\rho C(T) \cdot \left( \frac{\partial T}{\partial t} + \mathbf{v} \cdot \nabla T \right) = \mathbf{T} : \nabla \mathbf{v} + \mathbf{r} - \nabla \cdot \mathbf{q} \quad (2.12)$$

where  $C(T)$  is the dependence of heat capacity on temperature,  $r$  is the volumetric heat source,  $q$  is the heat flux, and  $\mathbf{T} : \nabla \mathbf{v}$  represents the viscous heating.

The extra stress tensor of (2.11) for a generalized Newtonian fluid in an isothermal flow is given by

$$\mathbf{T} = 2\mu \mathbf{D} \quad (2.13)$$

where  $\mathbf{D}$  is the rate of deformation tensor and  $\mu(\dot{\gamma})$  is the viscosity function of the local shear rate,  $\dot{\gamma}$ , as given in (2.14).

$$\dot{\gamma} = \sqrt{2tr(\mathbf{D}^2)} \quad (2.14)$$

The simplest form of the viscosity function is in the case of a Newtonian fluid, when it reduces to a constant value ( $\mu_0$ ) called Newtonian or zero-shear-rate viscosity. Examples of shear-dependent viscosity models used for polymeric liquids include the power-law model and the modified cross model (Prakash 1996);  $\mu$  can be calculated respectively as

$$\mu = m(\dot{\gamma})^{n-1} \quad (2.15)$$

$$\mu = \mu_0(1 + k\dot{\gamma})^{n-1} \quad (2.16)$$

For viscoelastic fluids, the extra stress tensor  $\mathbf{T}$  is divided into a viscoelastic part ( $\mathbf{T}_1$ ) and a purely viscous part ( $\mathbf{T}_2$ ), given by

$$A(\mathbf{T}_1, \lambda_t) \cdot \mathbf{T}_1 + \lambda_t \frac{\delta \mathbf{T}_1}{\delta t} = 2\eta_1 \mathbf{D}, \mathbf{T}_2 = 2\eta_2 \mathbf{D} \quad (2.17)$$

where the relaxation time  $\lambda_t$ , the viscosity factor  $\eta_I$ , and the function  $A(\mathbf{T}_1, \lambda_t)$  depend on the specific viscoelastic model used. The common differential viscoelastic models used to describe polymeric food materials are the Oldroyd-B, Maxwell, White-Metzner, Phan-Thien-Tanner, and Giesekus models (Connelly 2004).

## 2.4 Numerical Methods for Simulation of Mixing Flows

For a given system of fluid and mixing process, the solution of the above set of equations (consisting of conservation of mass and momentum), the energy equation (for non-isothermal problems), and the appropriate constitutive equations can be

obtained by several numerical techniques. The FEM is the most commonly used technique for numerical simulation of viscous mixing flows, even though other methods like the Finite Difference Method and the Finite Volume Method have been used (Dhanasekharan and Kokini 2003; Connelly and Kokini 2003; Heniche and Tanguy 2008).

Simulating a mixing flow using the FEM technique involves three steps:

- Construction of flow volume (or domain of flow problem) into a mesh made up of several finite elements or sub-domains
- Derivation of algebraic equations relating the physical quantities between the element nodes
- Solving whole flow domain: assembling equation parts using continuity and/or balancing the physical quantities across the elements (Reddy 2006)

The mesh generation step requires the construction of the mixing flow domain geometry using a network of linear triangular and quadrilateral elements (2D) or hexahedral, prism, tetrahedron, and wedge elements (3D). Several Computational Fluid Dynamics (CFD) software suites include mesh generation software, for example the Gambit (ANSYS Inc., Lebanon, NH) mesh generator. While maintaining the coarseness of the mesh is important in keeping the computational costs low, a higher density of finer mesh elements is needed in areas involving high gradients of flow properties. Hence, it is important to strike a balance with the coarseness/fineness of the mesh depending on the available computational capabilities. Additionally, for a higher accuracy and quicker convergence of the solution, the transition from coarser to finer mesh element regions has to be smooth and the individual elements as close as possible to ideal shapes, for example square/equilateral shapes (Connelly 2004; Heniche and Tanguy 2008). In the next step, the governing equations of motion are discretized using a weighted residual method and approximation of the flow variables for each element. For a generalized Newtonian fluid, the velocity, pressure, and stress fields (in case of viscoelastic flows) are approximated using the following equations

$$\mathbf{v}^h = \sum \mathbf{V}^i \psi_i \quad (2.18)$$

$$p^h = \sum p^i \pi_i \quad (2.19)$$

$$\mathbf{T}^h = \sum \mathbf{T}^i \phi_i \quad (2.20)$$

where  $\psi_i$ ,  $\pi_i$ , and  $\phi_i$  are the finite element basis functions and  $V_i$ ,  $p_i$ , and  $T_i$  are the nodal variables.

There are several methods available to discretize the governing equations, for example the Galerkin, the pressure stabilized Petrov-Galerkin, and the Galerkin least-square methods. In the Galerkin method, assuming the inertia terms to be negligible, the set of finite element equations in the flow domain  $\Omega$  are formulated as

$$\int_{\Omega} \pi_k [\nabla \cdot \mathbf{v}^a] d\Omega = 0 \quad (2.21)$$

$$\int_{\Omega} \left\{ \psi_j \rho \left[ \frac{D\mathbf{v}^a}{Dt} - \mathbf{f} \right] + \nabla \psi_j^T \cdot [-p^a \mathbf{I} + 2\eta^2 \mathbf{D}^a + \mathbf{T}_1^a] \right\} d\Omega = \int_{\Omega} \psi_j \sigma \cdot \mathbf{n} ds \quad (2.22)$$

$$\int_{\Omega} \phi_i \left[ g(\mathbf{T}_1) \cdot \mathbf{T}_1^a + \lambda \frac{\delta \mathbf{T}_1}{\delta t} - 2\eta_1 \mathbf{D}^a \right] d\Omega = 0 \quad (2.23)$$

For differential viscoelastic models, this system of equations can be solved by using a coupled method where the extra stress tensor is the primary variable along the pressure and velocity fields; the Newton–Raphson technique can be used to solve for the variables. In this method, one usually encounters a large number of unknowns and high computational costs. Another method often used is the decoupled method where the viscoelastic stress tensor is computed separately from the flow kinematics; the method is iterated using the Picard scheme. The accuracy and stability of Galerkin formulations deteriorates in viscoelastic flow problems as the elasticity number increases; thus further stabilization techniques such as streamlined upwind (SU) and elastic-viscous-stress splitting (EVSS) are needed. The reader is directed to literature by Connolly (2004) and references therein for a detailed review of these techniques.

Several commercial FEM simulation packages are available, such as FIDAP (ANSYS, Inc.), AcuSolve (Acusim Software), Polyflow (ANSYS, Inc.), and Poly3D (Rheosoft). In particular, the Polyflow suite, which includes a mesh generator (Gambit), an FEM solver (Polyflow), and a post-processor (Fluent-Post/Fieldview/CFX Post), has been extensively used by our group to simulate viscous and viscoelastic flows in mixers and extruders.

Solving for the flow in a mixing device using a CFD simulation package would include the following steps:

- Building mixer geometry and converting into FEM mesh using a mesh generator (e.g., Gambit)
- Defining flow boundaries, material properties, numerical parameters, and operating conditions
- Solving of velocity profiles using an FEM solver (e.g., Polyflow)
- Calculating various mixing measures from velocity data using a post processor (e.g., Fluent-Post/Fieldview/CFX-Post)

Simulation of mixers with geometry that varies continuously with time, as in the case of moving impellers or screw/paddle elements, requires special meshing techniques. One approach that can be applied to a single impeller or a single screw mixer is the “rotating reference frame technique” in which the impeller/screw becomes the fixed reference frame with the barrel rotating around it. This enables the flow domain mesh to be fixed in time. The velocities are then

transformed back to the inertial reference frame. In asymmetrical mixer geometries, as in the case of an eccentrically placed impeller or a twin screw continuous mixer design, a “mesh superposition technique” (MST) can be used in which the impeller or the screw/paddle elements are meshed separately from the flow domain and then superimposed (Connelly and Kokini 2006a). Here, the equation of motion is modified by the introduction of a penalty term ( $H$ ) to distinguish the solid (impeller or paddle) mesh elements from the fluid elements:

$$H(\mathbf{v}-\mathbf{v}) + (1-H)(-\nabla P + \nabla \cdot \mathbf{T} + \rho \mathbf{g} - \rho \mathbf{a}) = 0 \quad (2.24)$$

The penalty term  $H$  is essentially a step function and is set to a value of 1 for all nodes on solid moving parts, and a value of 0 for all nodes in the fluid volume. The continuity equation is also modified with a relative compression factor  $\beta$  to account for conservation of mass in the regions of flow domain covered by the moving solid elements:

$$\nabla \cdot \mathbf{v} + \frac{\beta}{\mu} \Delta P = 0 \quad (2.25)$$

## 2.5 3D Numerical Simulation of Model Mixing Geometries

In this section we present a review of studies evaluating the efficiency of distributive and dispersive mixing in model batch and continuous mixing geometries using numerical simulation techniques. These studies examined the effects of mixer operating parameters like screw design, screw speed, and material rheology on the variations in flow and mixing profiles. Recent studies in the area of numerical simulation and CFD of mixing processes can be broadly classified based on the mixing geometries investigated, for example, stirred tank reactors (Zalc et al. 2001, 2002a; Alvarez-Hernández et al. 2002; Rivera et al. 2004, 2006; Barailler et al. 2006; Iranshahi et al. 2006, 2007), dough kneaders (Jongen 2000; Jongen et al. 2003; Connelly and Kokini 2004, 2006a,b, 2007), static mixers (Rauline et al. 2000; Zalc et al. 2002b, 2003; Heniche et al. 2005), and continuous mixers/extruders (Dhanasekharan and Kokini 2000, 2003; Wang and Manas-Zloczower 2001).

### 2.5.1 Stirred Tank Reactors/Batch Mixers

Mixing of viscous liquids in stirred tank reactors and impeller-based batch mixers is widely employed in many process industries where effective distribution of additives is of great importance. Impeller design and speed of the impeller (as quantified



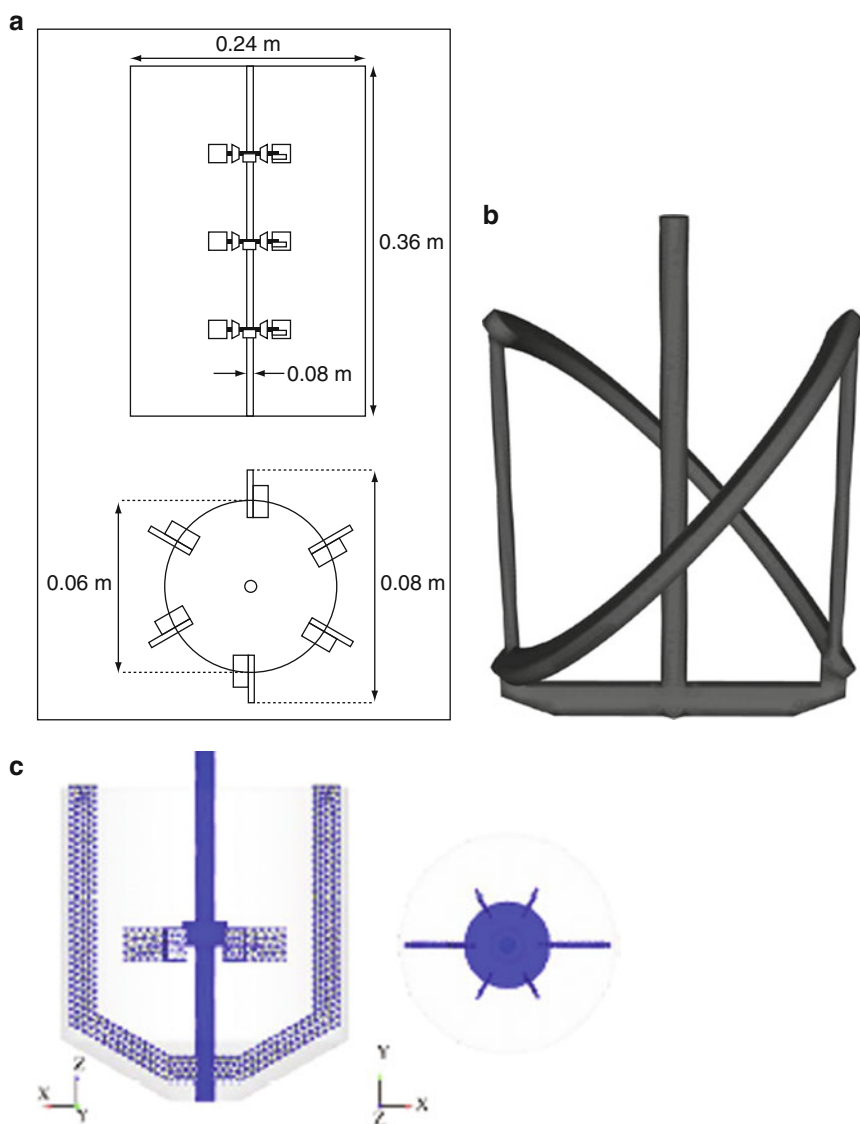


**Fig. 2.1** Examples of impeller designs in batch mixers: (a) Three-Rushton turbine (Zalc et al. 2001); (b) Paravisc impeller (Iranshahi et al. 2006); (c) Rushton turbine with coaxial anchor (Rivera et al. 2006)

by Reynold's number,  $Re$ ) are the major operating variables that can be tweaked to attain optimum mixing conditions and power efficiency. Figure 2.1 shows a few of the impeller designs used in stirred tank reactors and impeller-based mixers. The geometrically simple and symmetrical construction of the impellers, coupled with a relatively large flow volume in the reactor/vessel (usually cylindrical), makes these

mixers an excellent choice for use of CFD in the calculation and visualization of the various mixing measures as well as their validation using imaging techniques like the PIV.

Laminar mixing in a three-Rushton turbine stirred tank reactor was studied using the ORAC CFD package (Dantec Dynamics, Mahwah, NJ) (Zalc et al. 2001, 2002a) (Fig. 2.1a). The flow measurements were validated with PIV experiments using planar laser-induced fluorescence. In Fig. 2.2 the simulation results are in excellent agreement with the experiments in revealing the size and location of poorly mixed regions in the mixer. Local mixing efficiency can be quantified and visualized by computing the stretching value ( $\lambda$ ). The stretching value  $\lambda$  is calculated from deformation of infinitesimal vectors in the flow, which usually takes place at an exponential rate in chaotic flow regions as compared to a linear rate in non-chaotic flows. The contour maps of the logarithm of stretching shown in Fig. 2.3 reveal the spatial heterogeneity of stretching when mixing at various impeller speeds after 20 revolutions. Knowledge of the distribution patterns of stretching could be valuable in deciding the injection point for additives to achieve optimal distribution (Zalc et al. 2002a).

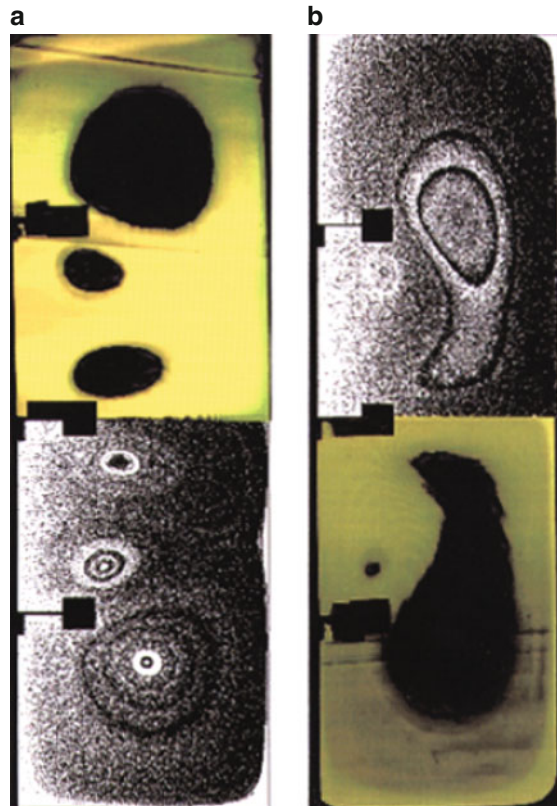


**Fig. 2.2** Comparison of experimental and simulated results showing excellent agreement in the mixing patterns in a three-Rushton turbine impeller mixer after 600 revolutions at (a)  $Re = 20$ ; and (b)  $Re = 40$  (Zalc et al. 2002a)

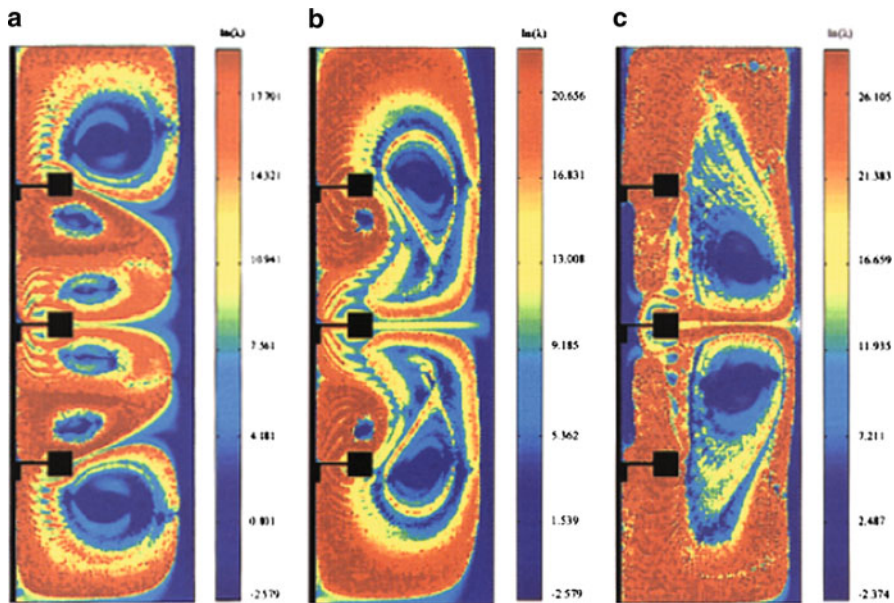


**Fig. 2.3** Contour plots of  $\ln(\lambda)$  reveal the spatial heterogeneity of stretching at various impeller speeds: (a)  $Re = 20$ ; (b)  $Re = 40$ ; (c)  $Re = 160$  (Zalc et al. 2002a)

In order for a mixing process to deliver optimum distributive and dispersive mixing, the entire set of operating conditions needs to be considered, that is, the impeller design, impeller speed, fluid rheology, and the injection point for additives. While comparing the mixing performance of an Ekato Paravisc impeller with a Double Helical Ribbon (DHR) impeller (Fig. 2.2b), Iranshahi et al. (2006) showed that the Paravisc impeller was more sensitive to the injection point chosen for a tracer in the effective distribution of the tracer particles in a Newtonian fluid (Fig. 2.4).

An important criterion for many mixing processes is the balance between distributive and dispersive mixing. Rivera et al. (2006) defined a parameter that is a ratio between two dimensionless quantities, the “head number”  $N_h$  (representing the shearing ability of the impeller) and the “flow number”  $N_q$  (representing the pumping ability of the impeller). The effect of an anchor co-rotating and counter-rotating with a Rushton turbine (Fig. 2.2c) was studied for a Newtonian and a non-Newtonian fluid by simulating the flow and mixing process, using POLY3D<sup>TM</sup> (Rheosoft, Inc.) finite element software. It can be seen from Table 2.1 that the co-rotating anchor was more effective in combined distribution and dispersion, while the counter-rotating anchor was poor at distribution. The poor distributive mixing with the counter-rotating mode can be visualized in Fig. 2.5, which shows the intensity of segregation of tracer particles (a measure of homogeneity of the mixing) at two different mixing times. Rivera et al. (2006) refer to this figure as “tracer dispersion,” whereas the actual process measured by the

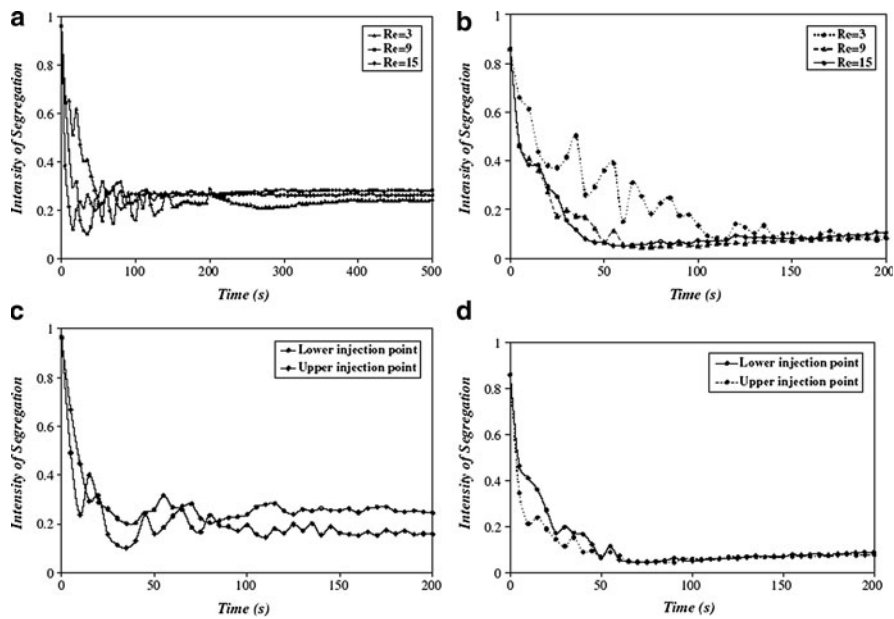


**Fig. 2.4** Intensity of segregation vs. time used for different *Re* and points of injection of tracer (Iranshahi et al. 2006)

**Table 2.1** Comparison of shearing and pumping abilities of the coaxial mixer for different rotating modes and fluid rheology (Rivera et al. 2006)

Operating conditions	$N_q$	$N_k$	$N_h/N_q$
Co-rotating Newtonian fluid	0.917	1.546	1.685
Rushton impeller only Newtonian fluid	0.658	1.474	2.477
Counter-rotating Newtonian fluid	0.756	1.631	1.948
Co-rotating non-Newtonian fluid	0.761	0.865	1.136
Rushton impeller only non-Newtonian Fluid	0.452	1.082	3.222
Counter-rotating non-Newtonian fluid	0.608	1.457	1.778

intensity of segregation is distributive mixing. Dispersive mixing in our definition relates to the breakup (e.g., of tracer drops) caused by the shearing action of the impellers. The rheology of the fluid also affected the efficiency of the mixing process in that the shear thinning of the viscosity resulted in smaller well-mixed areas.

**2.5.2 Dough Mixers and Kneaders**

Dough kneaders and mixers are designed for highly viscous doughs and batters that require actions that include pushing portions of the material through other portions, elevating, dropping and rotating the material, and cutting or dividing the material

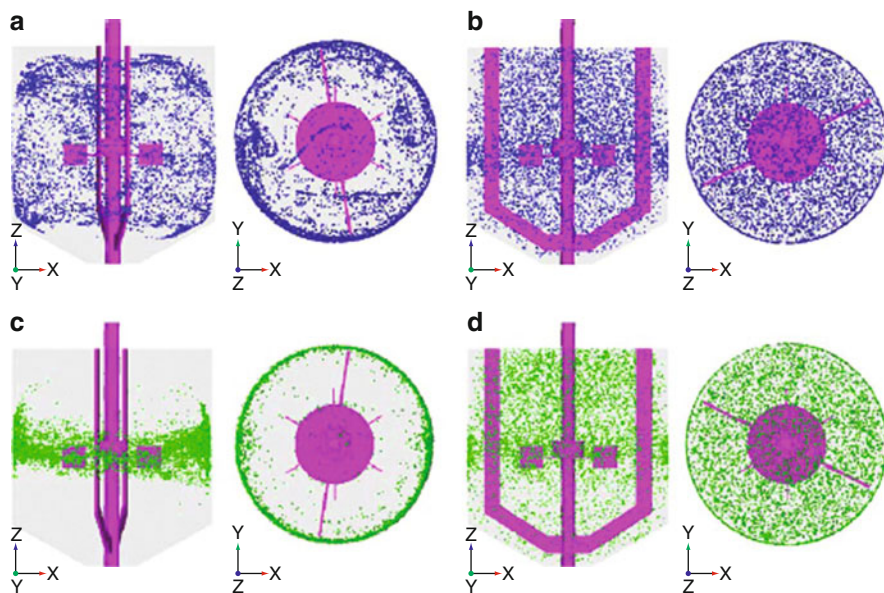


**Fig. 2.5** Distributive mixing in a Rushton turbine impeller with a coaxial anchor: (a) co-rotating after 15 s; (b) co-rotating after 150 s; (c) counter-rotating after 15 s; (d) counter-rotating after 150 s (Rivera et al. 2006)

(Connelly 2004). Most dough mixers are hence built to operate horizontally, and typically use co-rotating twin blades or arms like roller bars, single and twin sigma blades, open paddle four-way blades, double-arm blades, and spindle geometries. However, several smaller batch dough kneaders with Z blades, sigma blades, or rotating arms are used for empirical dough testing in laboratories. Examples include the plastograph (also called a farinograph) with two counter-rotating but non-intermeshing blades inside a closed cavity; the do-corder with two intermeshing blades co-rotating in a bowl, with limited clearance at the bowl wall; the planetary mixer (or mixograph) with mixing caused by the planetary motion of a rotating arm attached with a pair of vertical pins on either end; and the Eberhart spiral mixer with a spiral rod rotating in a bowl (Jongen et al. 2003) (Fig. 2.6).

Research aimed at optimizing batch kneaders involves experimental methods relating the operating parameters of these mixers to the dough development, rheology, and sensory quality of the product sample. Only a few studies were able to gather specific information on the flow profiles and mixing parameters due to the inherent difficulties with experiments (Prakash et al. 1999; Prakash and Kokini 2000). However, due to the recent advances in the design and simulation capabilities of various CFD software packages, specifically those aimed at viscous and viscoelastic flows, it is now possible to obtain (in a nonintrusive way) detailed information on flow and mixing parameters that includes distribution, dispersion, and laminar stretching in dough mixing.

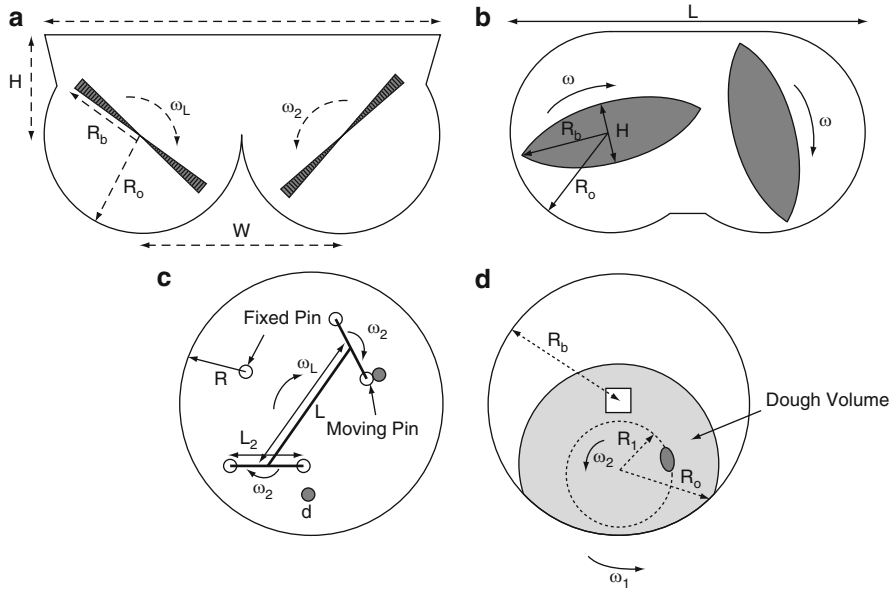


**Fig. 2.6** Dough kneaders of various geometries: (a) Farinograph; (b) Do-corder; (c) Mixograph; (d) Spiral mixer (Jongen et al. 2003)

Jongen et al. (2003) used a virtual FEM to study the deformation of viscous pastes in four different batch mixing geometries (Fig. 2.6). The technique involved superimposing the moving elements on the flow domain FEM mesh with the FIDAP (Ansys Inc., Lebanon, NH) FEM software. In order to quantify the deformation of the material, a flow parameter  $R^2$  was defined as the ratio of the second invariants of the shear rate and vorticity rate tensors. The normalized value of  $R^2$  was calculated as:

$$D = \frac{1 - R^2}{1 + R^2} \quad (2.26)$$

A comparison of the cumulative time-averaged frequency function for the three types of mixers (Fig. 2.7) showed that the spiral mixer had the most rotational flow; the do-corder the most elongational flow character; and the planetary mixer and plastograph the highest (approximately) shear to the material. An investigation of the same parameter at different operating conditions in the plastograph showed that, while rotational speed of the blades and gap clearance did not affect the type of deformation (value of  $D$ ), a change in the blade design helped reduce the rotational character of the mixing profile.

A more in-depth and detailed analysis of the 3D flow and mixing profiles in the Brabender® farinograph was performed by Connelly and Kokini (2006a, b) using MST in which the moving sigma blades and the barrel volume were separately meshed and superimposed. An FEM along with the MST was implemented in the



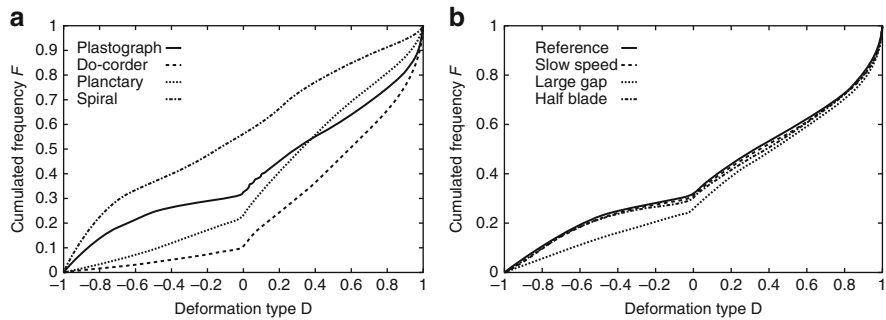


**Fig. 2.7** (a) Cumulative distribution of mean flow-type parameter  $D$  for various kneader geometries; (b) cumulative distribution of mean flow-type parameter  $D$  for a farinograph at different blade configurations and speeds (Jongen et al. 2003)

Polyflow<sup>®</sup> CFD software (ANSYS Inc., Lebanon, NH). Figure 2.8 shows the effect of fluid rheology on the velocity contour maps on the vertical center plane between the two blades. Increased shear thinning of the fluid caused a decrease in the velocity of the fluid right above the blades. The dispersive mixing ability was calculated as defined by (2.8). A histogram of the distribution of the dispersive mixing index in the central planes between the farinograph blades for the three fluids shows a decrease in the elongational flow regions with increasing shear thinning. The paths of material points can be calculated from the velocity profiles, which can then be used to evaluate the distributive and stretching efficiency parameters such as the cluster distribution index, scale of segregation, and the mean length of stretch. The density of probability of the length of stretch experienced by 10,000 infinitesimal material lines in the farinograph (Fig. 2.9) for three blade revolutions showed a gradual and steady increase in the amount of material undergoing effective stretching over time.

Limited work has been done on studying the effect of a fluid's viscoelasticity on flow and mixing profiles. Connelly and Kokini (2003) simulated the flow of a Phan-Thien Tanner fluid model in a 2D single screw mixer using a rotating reference frame technique; they compared different methods of handling the instabilities in dealing with a differential viscoelastic fluid model. It was found that the effect of viscoelasticity (an increase in relaxation times) was to create asymmetry in the velocity and pressure profiles and to reduce the effects of shear thinning on the pressure and stresses (Fig. 2.10).

### 2.5.3 Continuous Mixers and Extruders

Simulation of continuous mixer geometries requires increased computational costs due to the complexity and lack of symmetry in the geometry. The most common continuous screw-type mixer and extruder design used in the food industry is the

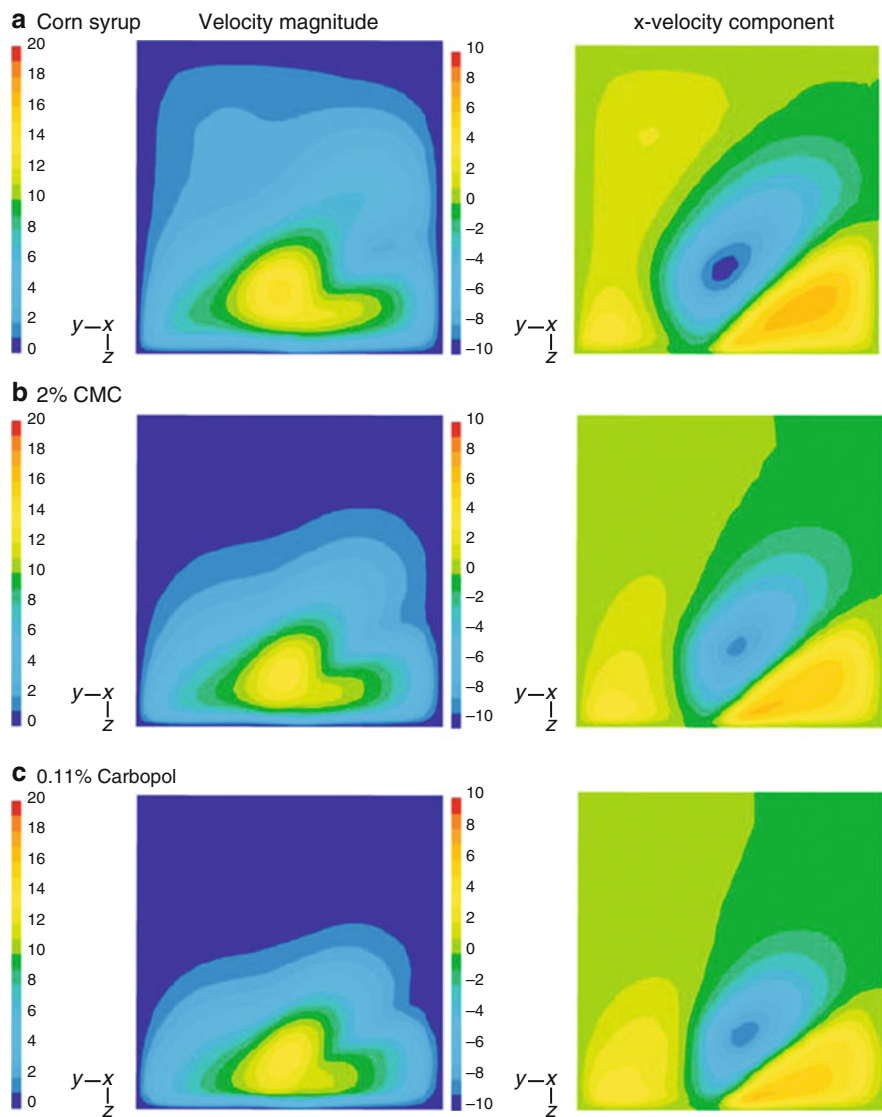


**Fig. 2.8** Effect of fluid rheology on the velocity profiles in the vertical center plane of a farinograph (Connelly and Kokini 2006a)

two-lobed twin-screw co-rotating design, for example the Readco<sup>®</sup> continuous mixer shown in Fig. 2.11. The design consists of a pair of co-rotating shafts fitted with a series of conveying screws, two- or three-lobed kneading blocks that can be staggered followed by discharge screw elements. There have been several analytical, experimental, and numerical studies conducted to decipher the flow and mixing patterns in both the conveying screw regions and the kneading region. As a first step



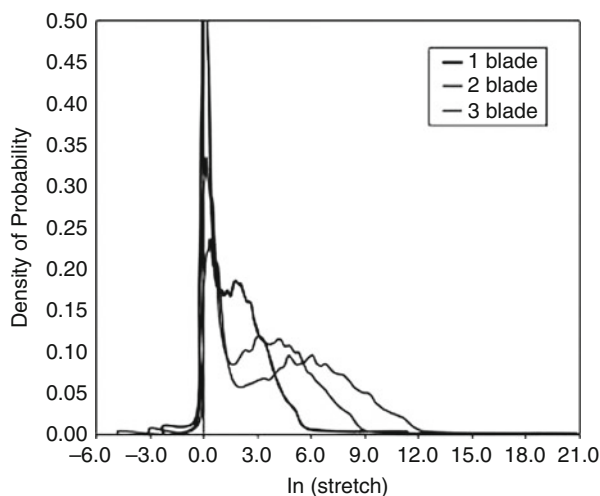


**Fig. 2.9** Density of probability for length of stretch  $\ln(\lambda)$  experienced by 10,000 infinitesimal material lines in a farinograph (Connelly and Kokini 2006b)

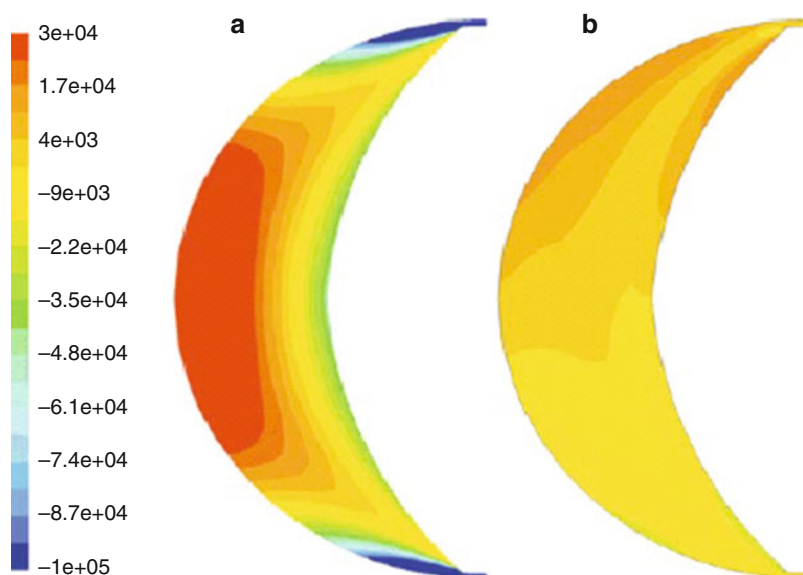


**Fig. 2.10** Shear stress ( $\text{g}/\text{cm}^2$ ) contour maps for fluid with relaxation times of (a) 0 s and (b) 100 s in a 2D single-paddle mixer (Connelly and Kokini 2003)

to studying the twin-screw continuous mixer design, Connelly and Kokini (2007) used numerical simulations to compare mixing of a Carreau model fluid in both a 2D single-paddle mixer and a 2D twin-paddle mixer. The presence of a second paddle element in the twin-screw geometry significantly improved both dispersive

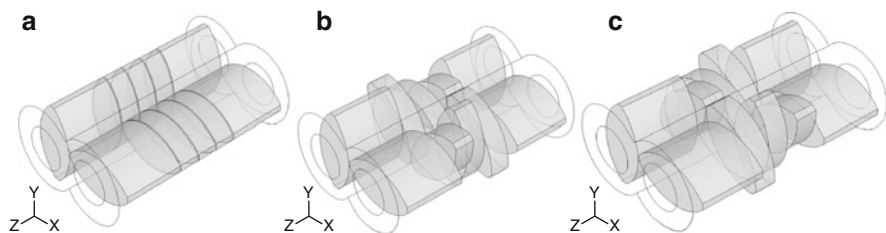


**Fig. 2.11** Kneading elements of the Readco<sup>®</sup> twin-screw processor (Readco Inc., York, PA) arranged in (a) FLAT, (b) 45F, and (c) 45R configurations (Vyakaranam and Kokini 2008)

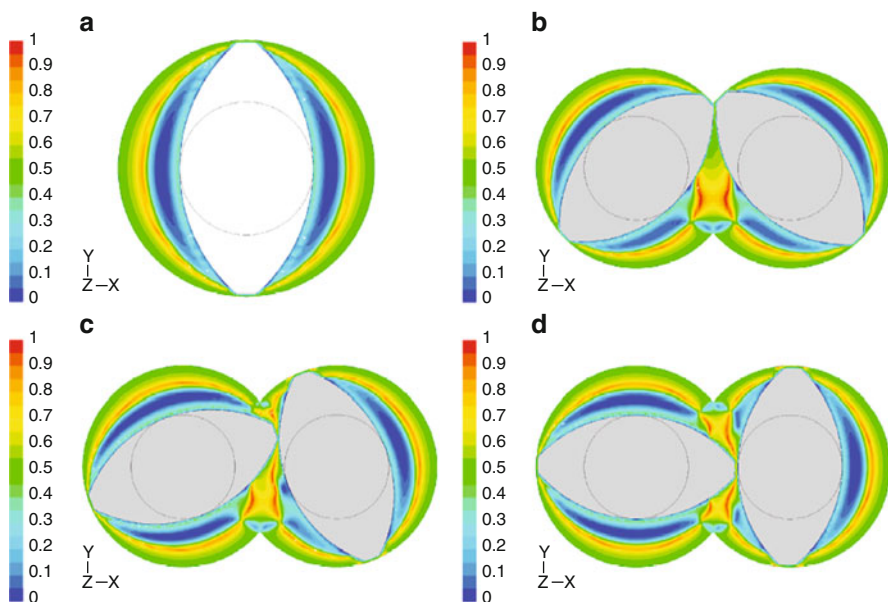


**Fig. 2.12** Mixing index ( $\lambda_{MZ}$ ) contours for the (a) single-screw and twin-screw mixers after rotation of the paddles at (b) 45°, (c) 67.5°, and (d) 90° (Connelly and Kokini 2007)

and distributive mixing. Figures 2.12 and 2.13 shows the dispersive mixing index and the cluster distribution index in both mixers. While the twin-screw geometry shows an increase in the area and magnitude of elongational flow, the single-screw geometry showed a cyclic cluster distribution index, suggesting that the material points were unable to leave the streamlines, leading to poor distributive mixing.

While these simulations were useful in showing the positive effect of a twin-paddle element on the mixing, 3D simulations of the full-length mixer are needed for a realistic simulation of continuous mixing, which involves axial flow. The study of continuous mixers is mainly focused on evaluating the effects of screw speed, stagger angle, and thickness of the paddle elements on the dispersive and distributive mixing measures, and comparing the performance to a batch mixer.

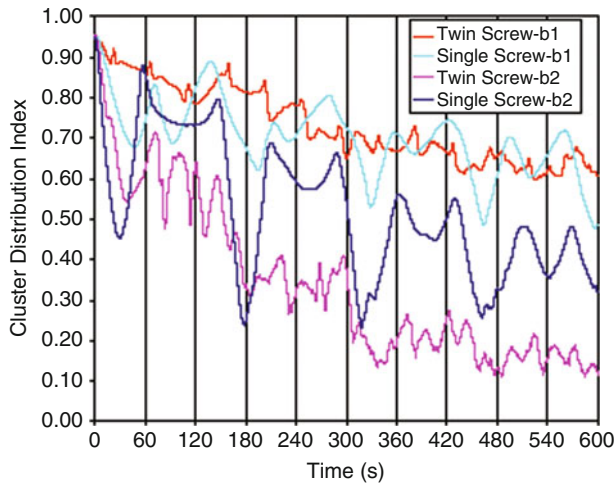


**Fig. 2.13** Comparison of cluster distribution index for ten revolutions in the single-screw and twin-screw mixers with different locations for the initial cluster in the flow domain: b1 (center location) and b2 (leftmost location) (Connelly and Kokini 2007)

For example, consider the 3D numerical simulation of the mixing of a generalized Newtonian fluid in a full-length kneading section of the Readco® continuous processor with nine paddle pairs. The flow data were evaluated for every  $10^\circ$  of movement by the paddles for ten rotations at three different screw speeds (1, 50, and 100 RPM); next the various distributive and dispersive mixing measures were evaluated. The paddle elements were staggered forward and reversed at an angle of  $45^\circ$  (Fig. 2.11).

Figure 2.14 shows the effects of screw speed and stagger angle on the time-averaged efficiencies of the three continuous mixer geometries in comparison with the farinograph. The time averaged instantaneous mixing efficiency decreased with increasing screw speed, with highest efficiency at the lowest screw speed of 1 RPM, which has been attributed to higher residence time of the material at lower screw speed resulting in greater stretching and folding of the material. The FLAT (or neutral, with no element stagger) configuration showed the highest efficiency (Ashokan 2008).

Mixing efficiency is also affected by the individual paddle element width and the increase in the number of gaps between the elements, as a result of increasing the number of elements. Figure 2.15 shows the area stretch (as a measure of distributive mixing) of different kneading element widths for two-lobe kneading elements. The smaller the disc width, the better was the area stretch; it was hypothesized that the increase in the number of gaps caused an increase in the area stretch (Ishikawa et al. 2001).

Yoshinaga et al. (2000) studied the isothermal flow of a Carreau model non-Newtonian fluid in the kneading section of a twin-screw extruder using FEM

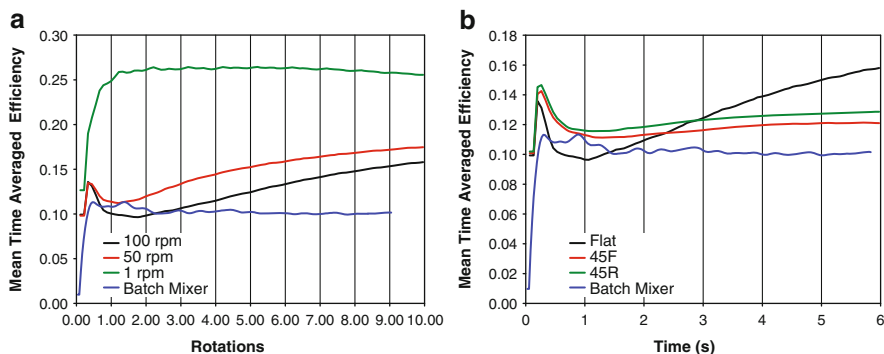
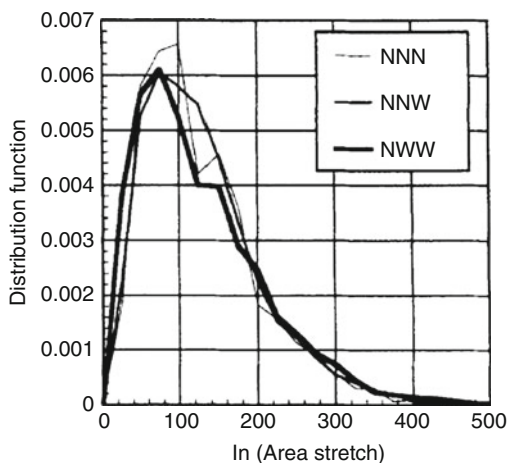


**Fig. 2.14** Effect of (a) screw speed and (b) screw configuration on time-averaged mixing efficiency of the Readco<sup>®</sup> twin-screw continuous mixer and the farinograph batch mixer (Ashokan 2008)

**Fig. 2.15** Distribution of the area stretch in mixing region of a co-rotating twin-screw extruder for different kneading disc widths (i.e., NNN, NNW, and NWW) (Ishikawa et al. 2001)



simulations. The shafts were fitted with five pairs of three-lobed mixing elements configured at different stagger angles. Distributive mixing was measured by residence time distributions and the minimum distance between mass-less particle markers after mixing for a given time. The simulations were performed as a quasi-steady state wherein the velocity profiles were calculated for every  $3^\circ$  of rotation of the screw elements. Both the residence time distributions and the mean nearest distance between the markers showed the neutral stagger configuration to be the most beneficial for distributive mixing (Fig. 2.16).

Dispersive mixing can be analyzed by evaluating the dispersive mixing index and corresponding shear stresses (or shear rates, if a Newtonian fluid). Figure 2.17 shows the contour maps of shear rate and mixing index ( $\lambda_{MZ}$ ) at the 1st, 4th, and 8th

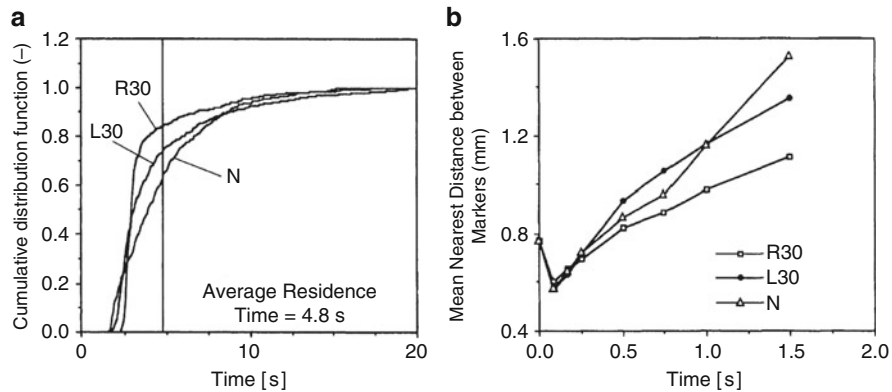


**Fig. 2.16** (a) Residence time distribution and (b) mean nearest distance between markers in mixing region of a co-rotating extruder fitted with three-lobed kneading discs (Yoshinaga et al. 2000)

paddle elements of the FLAT configuration for a Newtonian fluid mixed at 75 RPM. The elongational flow, indicated by the red shade, is the highest in the center region of the mixer (around the 4th paddle element), while highest shear rates are found in the intermeshing regions. The elongational flow is known to cause a breakup of agglomerates and drops in flow; the corresponding shear rate can be made dimensionless by using the capillary number ( $Ca$ ). The  $Ca$  can be defined as the ratio of the viscous forces acting to deform the drop to the interfacial forces resisting deformation and acting to restore its spherical shape. At high enough  $Ca$ , the drop deformation becomes unsteady, leading to breakup. The equation for  $Ca$  is given as:

$$Ca = \frac{\mu \dot{\gamma}}{\sigma} r \quad (2.27)$$

where  $\mu$  is the viscosity of the continuous medium (food matrix),  $\dot{\gamma}$  is the local shear rate,  $r$  is the bubble radius, and  $\sigma$  is the surface tension of the food matrix (Meijer and Janssen 1994; Risso 2000). The effect of paddle element stagger on the distribution of  $Ca$  and  $\lambda_{MZ}$  for air bubbles in a Newtonian corn syrup is shown in Fig. 2.18 for the FLAT, 45F (with a 45° forward element stagger), and the 45R (with a 45° reverse element stagger) configurations. It can be seen that the density of points in the mixer with  $Ca$  and  $\lambda_{MZ}$ , which are high enough for breakup, decreases with a reverse stagger angle of the paddle elements, suggesting higher breakup in the FLAT configuration. The effects of stagger angle and screw speed on the shear stresses (or  $Ca$ ) and distribution of flow type give useful information that aids in the design of mixers with better dispersive abilities.

Numerical simulation of the flow of fluids modeled by a viscoelastic constitutive equation in a complex 3D geometry is a nontrivial task. For example, the MST

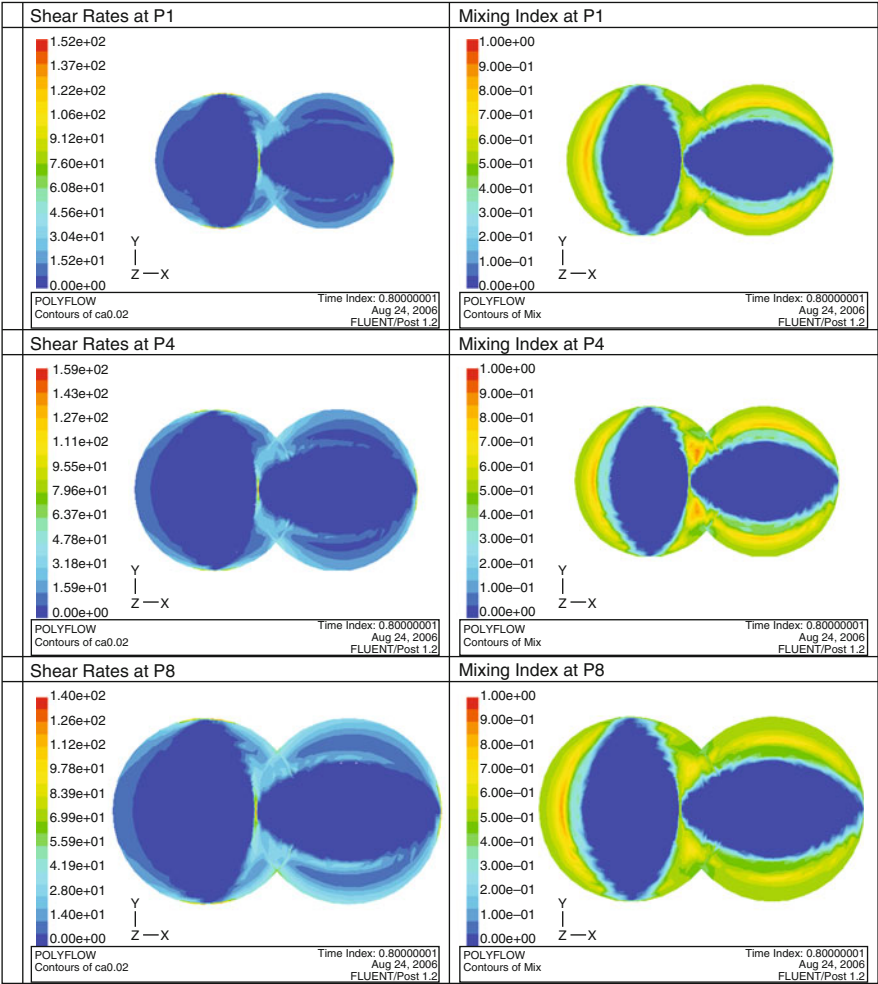


**Fig. 2.17** Distribution of shear rate ( $\dot{\gamma}$ ) and mixing index ( $\lambda_{MZ}$ ) at different locations in the twin-screw mixer at a screw speed of 75 RPM (Vyakaranam and Kokini 2008)

technique in the POLYFLOW FEM solver does not support the use of a viscoelastic constitutive equation; therefore a new technique is needed to model the fluid flow. One such technique is the Pseudo Steady State (PSS) technique in which the flow is modeled as a steady state with the viscoelastic constitutive equation for a snapshot of the moving geometry; the velocity, pressure, and stress results are then used as the input for successive time steps (Ishikawa et al. 2001). Preliminary demonstration of the technique using a 2D Readco<sup>®</sup> geometry was successful in obtaining the velocity and shear rate profiles at low Deborah numbers and small rotations of the paddle elements (Ashokan 2008). Further work is needed to extend the simulation

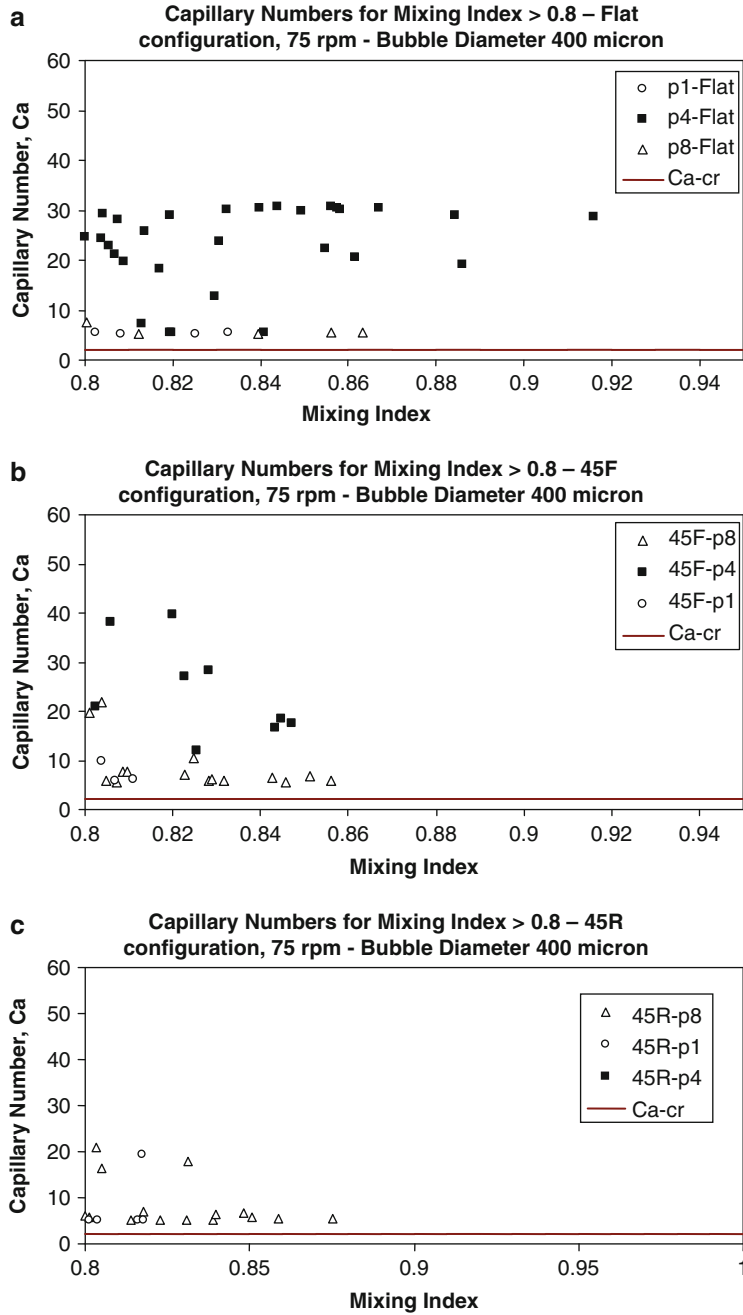


**Fig. 2.18** Distribution of  $Ca$  and  $\lambda_{MZ}$  values for all calculated points in mixing region of the Readco<sup>®</sup> twin-screw mixer at different screw configurations (Vyakaranam et al. 2009)

of viscoelastic simulations in full 3D geometry at higher Deborah numbers and larger rotations of the paddles.

## 2.6 Conclusions

Recent studies in numerical simulation of viscous flow and mixing in the laminar regime have shown the FEM to be a cost-effective and nonintrusive technique for analyzing and visualizing the distributive and dispersive mixing ability in batch and continuous mixing devices of various geometries. A review of recent work analyzing the mixing of viscous and viscoelastic fluids using numerical simulations has been presented. Stirred tank reactors and batch mixers of varying geometries have been successfully employed to demonstrate the use of numerical simulations for visualization and analysis of viscous and viscoelastic mixing in 3D. While the simulation of flow and mixing for fluids of relatively simple rheological character (viscous Newtonian and non-Newtonian) has been done for complex geometries at a 3D level, there is a need for further work in simulating the mixing of more complex viscoelastic fluid models in full-scale continuous mixer geometries.

**Acknowledgments** The authors would like to thank Dr. Nesli Sozer for help with proofreading the document.

## References

- Alvarez-Hernández MM, Shinbrot T, Zalc J, Muzzio FJ (2002) Practical chaotic mixing. *Chem Eng Sci* 57(17):3749–3753
- Ashokan BK (2008) Developing methods for design and analysis of continuous mixers through 3D numerical simulation of flow and mixing, Ph.D. thesis. Food Science, Rutgers University
- Barailler F, Heniche M, Tanguy PA (2006) CFD analysis of a rotor-stator mixer with viscous fluids. *Chem Eng Sci* 61(9):2888–2894
- Bentley BJ, Leal LG (1986) An experimental investigation of drop deformation in steady, two-dimensional linear flows. *J Fluid Mech* 167:241–283
- Connolly RK (2004) Numerical simulation and validation of the mixing of dough-like materials in model batch and continuous dough mixers, Ph.D. thesis: 430. Food Science, Rutgers University
- Connolly RK, Kokini JL (2003) 2-D numerical simulation of differential viscoelastic fluids in a single-screw continuous mixer: application of viscoelastic finite element methods. *Adv Polym* 22(1):22–41
- Connolly RK, Kokini JL (2004) The effect of shear thinning and differential viscoelasticity on mixing in a model 2D mixer as determined using FEM with particle tracking. *J Non-Newtonian Fluid Mech* 123(1):1–17
- Connolly RK, Kokini J (2006a) 3D numerical simulation of the flow of viscous Newtonian and shear thinning fluids in a twin sigma blade mixer. *Adv Polym Technol* 25(3):182–194
- Connolly RK, Kokini J (2006b) Mixing simulation of a viscous Newtonian liquid in a twin sigma blade mixer. *AIChE J* 52(10):3383–3393



- Connelly RK, Kokini JL (2007) Examination of the mixing ability of single and twin screw mixers using 2D finite element method simulation with particle tracking. *J Food Eng* 79 (3):956–969
- Dhanasekharan M, Kokini JL (2000) Viscoelastic flow modeling in the extrusion of a dough-like fluid. *J Food Proc Eng* 23(3):237–247
- Dhanasekharan M, Kokini J (2003) Design and scaling of wheat dough extrusion by numerical simulation of flow and heat transfer. *J Food Eng* 60(4):421–430
- Grace HP (1982) Dispersion phenomena in high viscosity immiscible fluid systems and application of static mixers as dispersion devices in such systems. *Chem Eng Commun* 14:225
- Heniche M, Tanguy PA (2008) Finite element modeling of viscous mixing: a review. *Chem Product Process Model* 3(1):55
- Heniche M, Tanguy PA, Reeder MF, Fasano JB (2005) Numerical investigation of blade shape in static mixing. *AIChE J* 51(1):44–58
- Iranshahi A, Heniche M, Bertrand F, Tanguy PA (2006) Numerical investigation of the mixing efficiency of the Ekato Paravisc impeller. *Chem Eng Sci* 61(8):2609–2617
- Iranshahi A, Devals C, Heniche M, Fradette L, Tanguy PA, Takenaka K (2007) Hydrodynamics characterization of the Maxblend impeller. *Chem Eng Sci* 62(14):3641–3653
- Ishikawa T, Kihara S, Funatsu K (2001) 3-D non-isothermal flow field analysis and mixing performance evaluation of kneading blocks in a co-rotating twin screw extruder. *Polym Eng Sci* 41(5):840–849
- Jongen T (2000) Characterization of batch mixers using numerical flow simulations. *AIChE J* 46 (11):2140–2150
- Jongen TRG, Bruschke MV, Dekker JG (2003) Analysis of dough kneaders using numerical flow simulations. *Cereal Chem* 80(4):383–389
- Meijer MEH, Janssen JMH (1994) Mixing of immiscible liquids. In: Manas-Zloczower I, Tadmor Z (eds) *Mixing and compounding of polymers: theory and practice*. Carl Hanser Verlag, New York
- Muzzio FJ, Alvarez MM, Cerbelli S, Giona M, Adrover A (2000) The intermaterial area density generated by time- and spatially periodic 2D chaotic flows. *Chem Eng Sci* 55(8):1497–1508
- Ottino JM (1989) *The kinematics of mixing: stretching, chaos and transport*. Press Syndicate of University of Cambridge, Cambridge
- Prakash S (1996) Characterization of shear rate distribution in a model mixer using laser doppler anemometry. Ph.D. thesis: 315. Food Science, Rutgers University
- Prakash S, Kokini JL (2000) Estimation and prediction of shear rate distribution as a model mixer. *J Food Eng* 44(3):135–148
- Prakash S, Karwe MV, Kokini JL (1999) Measurement of velocity distribution in the Brabender farinograph as a model mixer, using laser-doppler anemometry. *J Food Process Eng* 22 (6):435–454
- Rauline D, Le Blévec JM, Bousquet J, Tanguy PA (2000) A comparative assessment of the performance of the Kenics and SMX static mixers. *Chem Eng Res Des* 78(3):389–396
- Reddy JN (2006) *An introduction to the finite element method*. Tata McGraw-Hill, New Delhi
- Risso F (2000) The mechanisms of deformation and breakup of drops and bubbles. *Multiphase Sci Technol* 12:1–50
- Rivera C, Heniche M, Ascanio G, Tanguy P (2004) A virtual finite element model for centered and eccentric mixer configurations. *Comp Chem Eng* 28(12):2459–2468
- Rivera C, Foucault S, Heniche M, Espinosa-Solares T, Tanguy PA (2006) Mixing analysis in a coaxial mixer. *Chem Eng Sci* 61(9):2895–2907
- Vyakaranam KV, Kokini J (2008) Study of the dynamics and size distributions of air bubbles during mixing in a continuous food mixer. In: Campbell G, Scanlon M, Pyle L (eds) *Bubbles in food 2: novelty, health and luxury*. AACC, St. Paul
- Vyakaranam KV, Evans ME, Ashokan BK, Kokini JL (2009) Evaluation of mixing and air bubble dispersion in viscous liquids using numerical simulations. In: Cullen PJ (ed) *Food mixing: principles and applications*. Wiley-Blackwell, Oxford

- Wang W, Manas-Zloczower I (2001) Temporal distributions: the basis for the development of mixing indexes for scale-up of polymer processing equipment. *Polym Eng Sci* 41 (6):1068–1077
- Yang H-H, Manas-Zloczower I (1992) Flow field analysis of the kneading disc region in a co-rotating twin screw extruder. *Polym Eng Sci* 32(19):1411–1417
- Yoshinaga M, Katsuki S, Miyazaki M, Liu L, Kihara S, Funatsu K (2000) Mixing mechanism of three-tip kneading block in twin screw extruders. *Polym Eng Sci* 40(1):168–178
- Zalc JM, Alvarez MM, Muzzio FJ, Arik BE (2001) Extensive validation of computed laminar flow in a stirred tank with three Rushton turbines. *AIChE J* 47(10):2144–2154
- Zalc JM, Szalai ES, Alvarez MM, Muzzio FJ (2002a) Using CFD to understand chaotic mixing in laminar stirred tanks. *AIChE J* 48(10):2124–2134
- Zalc JM, Szalai ES, Jaffer S, Muzzio FJ (2002b) Characterization of flow and mixing in an SMX static mixer. *AIChE J* 48(3):427–436
- Zalc JM, Szalai ES, Muzzio FJ (2003) Mixing dynamics in the SMX static mixer as a function of injection location and flow ratio. *Polym Eng Sci* 43(4):875–890

Food Engineering Interfaces

Aguilera, J.M.; Simpson, R.; Welte-Chanes, J.; Bermudez

Aguirre, D.; Barbosa-Cánovas, G.V. (Eds.)

2011, XVIII, 694 p., Hardcover

ISBN: 978-1-4419-7474-7